RSC Advances

PAPER

View Article Online
View Journal | View Issue

Cite this: *RSC Adv.*, 2024, **14**, 24373

Developing a new sustainable eco-adsorbent film from flexographic printing plate waste to remove cationic organic and inorganic pollutants†

Noha A. Elessawy, *[a] Abdulrahman G. Alhamzani, [b] Mortaga M. Abou-Krisha[b] and Saad Aljlil[c]

Although climate change poses a threat to the future of the world, we still have time to adapt and lessen its effects. However, the incineration of polymeric waste materials has increased the release of carbon-containing gases called greenhouse gases (GHGs) and tiny particles called 'black carbon', leading to global warming, which is the cause of the worst environmental crisis in history. Flexography is an advanced printing technique and is widely used in the packaging industry as well as in the printing of various functional films and coatings. In general, the polymeric waste produced from this industry poses a grave environmentally sustainable problem; thus, due to the fact that this waste's primary component is carbon, it has attracted our attention towards converting it into carbon-based value-added products such as graphene, which can be used in water treatment processes. The prepared material was tested as a potential coated film in a batch adsorption system for the removal of lead (Pb) and methylene blue (MB) after being supported on poly(vinyl alcohol) (PVA) film. Furthermore, contact time, solution pH, and starting pollutant concentrations were studied and used in the response surface methodology (RSM) model for optimization. The adsorption kinetics were more clearly depicted by the pseudo-second-order kinetic model. To meet the objectives of waste management and water treatment, waste-derived materials can be used in wastewater treatment, based on the "wastes-treat-wastes" approach.

Received 20th March 2024
Accepted 22nd July 2024

DOI: 10.1039/d4ra02111h

rsc.li/rsc-advances

1. Introduction

In the world of packaging, flexographic printing is a popular printing technique due to its high-speed printing capabilities dealing with large active areas and volumes that need to be printed. The market capacity for flexographic printing plates is growing rapidly and a massive amount of flexographic printing waste plates are produced annually, causing a serious environmental problem as the flexographic printing plate wastes have low bio- and photo-degradability, indicating very low degradability, taking at least thousands of years to degrade, releasing toxins into soil and water along the way. On the other hand, incineration of this waste will increase global warming. In line with global requirements to mitigate climate change, which is a threat to our planet's future, the use of flexographic printing waste plates wherein carbon is the major constituent of the waste that produces high-value-added products instead of incinerating the waste is a critical demand. Consequently, it will prevent the release of toxins into air, soil and water along the way, in addition to inhibiting the release of powerful greenhouse gases, such as CO_2 and methane, and other gases. This would thus slow down the rate of climate change and prevent the Earth from getting hotter. From this point of view, upcycling flexographic printing waste plates produced from the flexographic printing activity can be performed using catalytic pyrolysis to produce carbon-based materials,[1] which can be used in wastewater treatment.[2,3]

Chemical technology has advanced, enabling the synthesis and processing of organic compounds, which are the most harmful type of water contaminants that can cause harm to both human health and marine organisms. Cationic methylene blue dye (MB) is particularly notable among these toxins because it is very soluble in water and blocks sunlight, which is harmful to marine life. Additionally, it may have detrimental consequences on human health, including cyanosis, methemoglobinemia, seizures and tachycardia.[4] Despite the risks, MB is widely used in many industries, including food, printing, medicines, cotton, and wood. As such, it is imperative to cleanse the effluent from these companies before discharging it into the water system. Furthermore, other dangerous pollutants are heavy metals; nonetheless, Pb(II) ions are frequently detected in

[a]*Computer Based Engineering Applications Department, Inform Research Institute, Alexandria, Egypt. E-mail: nony_essawy@yahoo.com*

[b]*Chemistry Department, College of Science, Imam Mohammad Ibn Saud Islamic University (IMSIU), Riyadh 11623, Saudi Arabia*

[c]*Institute of Water Management & Treatment Technologies, King Abdulaziz City for Science and Technology (KACST), Riyadh 11442, Saudi Arabia*

† Electronic supplementary information (ESI) available. See DOI: https://doi.org/10.1039/d4ra02111h

soil, water, and air.[5,6] The maximum permissible limit of lead had been set for drinking water by the World Health Organization at 0.01 mg L^{-1} due to the metal's propensity to accumulate within living things, hence posing a risk to public health.

Different methods, including coagulation and flocculation,[7,8] biological,[9,10] chemical oxidation,[11] photocatalytic,[12] filtration techniques,[13] and adsorption procedures using either natural or synthetic materials,[14] which are used to extract many kinds of contaminants from polluted waters. On the other hand, the adsorption technique's low cost, straightforward design, and great efficiency make it a potential approach. Nevertheless, because cost is a crucial factor in comparing adsorbent materials, researchers have focused increasingly on low-cost adsorbents made from polymeric waste in the past ten years. But if the adsorbent has a plentiful supply and minimal processing needs, it might be referred to as "a low-cost adsorbent." Adsorbents at minimal cost have been successfully employed to remove heavy metals, dyes, and other emerging contaminants.[15–18] The proposed process to obtain carbon-based materials from flexographics printing waste plates has a number of advantages over conventional methods. This method is a simple method with easy operational procedure, reproducible, affordable process, environmentally friendly and offering great potential for industrial production.

Graphene and its derivatives or composites can effectively be used as adsorbents,[2,3] however, many studies have shown a correlation between the amount of oxidation on graphene and its adsorption capabilities[19] whereas graphene with a high degree of oxidation or having many active sites, has high hydrophilicity and that enhances its interaction with contaminants.[20]

A significant obstacle in the wastewater treatment process is the widespread separation and recycling of nanomaterials. A possible solution is the support of graphene on a polymeric matrix, such as polyvinyl alcohol (PVA). Polyvinyl alcohol (PVA) is a synthetic polymer that is water soluble, non-toxic, and has the ability to create films;[21,22] hence, the creation of adsorbent coated is gaining interest.

Accordingly, the present study aims to upcycle flexographics printing waste plates and produce value-added materials such as graphene oxide (GO), which is a demanding area as it has several benefits, including environmental sustainability, waste management and produce adsorbent materials with low cost that can be used in wastewater treatment. Additionally, research was conducted to create a brand-new, extremely efficient coated adsorbent and assess how effectively it removed lead (Pb) and methylene blue (MB) dye. Response surface methodology (RSM) is a statistical design that was used to minimise the number of tests, investigate the correlations between the response as a dependent variable and the effective elements as independent variables, and identify the ideal process's operating parameters. The safe disposal of hazardous environmental contaminants is the primary industrial application which is anticipated to result in the coated adsorbent as a viable option.

2. Materials and methods

2.1. Materials

PVA +99% was purchased from Sigma-Aldrich (St. Louis, MI, USA), glutaraldehyde (GA) (50 wt% in H_2O, Alfa Aesar, USA), the flexographic printing waste plates were provided by Inciflex Egypt for industry and trade Co.

2.2. Composite film synthesis

2.2.1. Preparation of graphene oxide (GO). GO was prepared by catalytically pyrolyzing waste from shredded flexographic printing plates in a closed stainless steel autoclave jar. The jar was then placed into an electric furnace and heated to 800 °C for 30 minutes. The final product was ground into a fine powder.

2.2.2. Preparation of GO@PVA coated film. After dissolving 10 g of PVA in deionized water at 90 °C for two hours until a clear solution was achieved, 1 mL of GA was added and the mixture was stirred for 2 h after which the solution was cast in a 15 cm Petri dish. Subsequently, the precise quantity of GO was combined with 5 mL of acetone and 2 mL of GA and sonicated for 30 minutes to ensure dispersion. For GO, three weight ratios 1, 2, and 3 wt% were employed. On the PVA semi-dry film, the GO solution was applied in a specific amount and allowed to dry fully over an interval of 24 hours. Fig. S1 in the ESI† film provides a schematic description of the entire process. The GO@PVA coated films were designated as GO_1@PVA, GO_2@PVA, and GO_3@PVA, depending on the GO ratio.

2.3. Characterization

The functional groups of PVA, GO, and GO@PVA coated films were characterized using Fourier transform infrared spectroscopy (FTIR) on a Bruker ALFA spectrometer, Germany. Raman study on GO was performed using a SENTERRA Raman spectrometer, Bruker, Germany with a laser beam of 514.5 nm. Scanning electron microscopy (SEM) was performed on a JSM-IT200-JEOL instrument, Japan, and transmission electron microscopy (TEM) was performed on a JEOL, JEM 1230 instrument, Japan to analyze the surface morphology. The hydrophilicity of the coated films was confirmed using a contact-angle analyzer, Rame-Hart Instrument Co. model 500-FI.

2.4. Adsorption tests

A batch equilibration method was used to conduct the adsorption experiments. Diluted standard solutions containing 1 g L^{-1} of MB or Pb were employed to provide a variety of MB dye and Pb concentrations (50, 100, 150, and 200 mg L^{-1}). The concentration of MB in the solution was measured using UV-visible spectroscopy at wavelengths of 650 nm, and the Inductive Coupled Plasma Mass Spectrometer (ICP-MS, Agilent 7700, USA) was used to measure the concentration of Pb residual in the solution. The formulas (1) and (2) were used to determine the adsorbed quantities.

$$q_t = \frac{C_0 - C_t}{m} V \quad (1)$$

$$q_e = \frac{C_0 - C_e}{m} V \quad (2)$$

where C_0, C_t, and C_e (mg L^{-1}) are the MB or Pb concentrations at the beginning time, time t, and the equilibrium time, respectively; q_t and q_e (mg g^{-1}) are the quantities of the MB or Pb adsorbed per unit weight of the coated film at time t and equilibrium time, respectively. The mass of the coated film is m (g); the volume of the MB or Pb solution is V (L). The removal efficiency (R%) was determined using the following formula:

$$R\% = \frac{C_0 - C_t}{C_0} \times 100 \quad (3)$$

The pH was set to 6 and the adsorption period was varied within a range of 5 to 120 minutes for kinetics research. The adsorption kinetics were carried out using the pseudo-first and second-order models.

2.5. Optimization of the adsorption process

Using the response surface methodology (RSM) model (STAT-EASE, INC.'s Design-Expert 13.0.9.0 software) a link between variables and responses was developed in order to optimize the conditions for the adsorption processes of the MB dye and Pb ions. With 17 trials, the chosen matrix for the RSM model adhered to the Box–Behnken design.[23] As shown in Table 1 for MB and Pb pollutants, three parameters were utilized to evaluate the efficacy of the adsorption process: A (duration time, min); B (initial concentration of MB or Pb, mg L^{-1}); and C (solution pH), at three levels of −1, 0, and 1. Analysis of variance (ANOVA) was utilized to statistically validate the created polynomial models, and the F-test was employed to assess their statistical significance and the coefficient of determination (R^2) was employed to assess the quality of the fit.[24]

2.6. Regeneration and recycling

50 mg of the GO@PVA coated film was placed into two conical flasks, one holding 25 mL of 50 mg L^{-1} MB solution and the other holding 25 mL of 50 mg L^{-1} Pb solution, in order to test the coated film's regeneration potential. The mixture was shaken for the optimum time at 150 rpm. Following the adsorption procedure, the coated film was separated *via* filtering. It was then sonicated for 30 minutes with a solution of 100 mL ethanol and 10 mL 0.1 M NaOH. Finally, it was filtered, cleaned, and dried at 40 °C for six hours before being reused. After that, the filter fluid's concentration was measured. The preceding steps were repeated five times.

Table 1 Levels of several independent variables at RSM experimental design coded values

		Coded levels		
Symbol	Independent variables	−1	0	1
A	Time/min	60	120	180
B	Initial concentration/mg L^{-1}	100	150	200
C	Solution pH	2	7	12

3. Results and discussion

3.1. Characterization of GO and nanocomposite films

For the prepared GO from the flexographic printing plates waste, the survey XPS spectrum shown in Fig. 1a, demonstrates two main peaks at the binding energy of 533.2 eV and 286.5 eV corresponding to the O 1s and C 1s peaks respectively. By curve-fitting analysis as shown in Fig. S2a in the ESI file,† the C 1s spectrum of GO was deconvoluted into five peaks at 283.9, 284.5, 285, 287 and 290 eV, corresponding to the sp^3 and sp^2 carbon in aromatic rings, C–O bond, the epoxide C=O and the carboxyl functional groups, respectively, which are the principal bonding types existing in GO and these align with earlier research.[25,26] Furthermore, as illustrated in Table 2 and Fig. S2b† the oxygenated functions can be identified from O–H, C=O, C–O, and C–O–C groups.

The FT-IR spectrum analysis was employed to examine differences in the adsorbent's functional groups. FT-IR spectrum for the GO is presented in Fig. 1b. The adsorption peaks around 3000–3700 cm^{-1} and 1043.97 cm^{-1} are indicative of the existence of the bonded hydroxyl groups from carboxylic groups, alcohol/phenol O–H stretch and H_2O. The peak around 1122 cm^{-1} corresponds to C–O stretching in ethers groups, however, the peak around 1623 cm^{-1} is due to the C=C in-plane vibrations or C=O in the carbonyl and carboxyl groups which accorded well with the previous works.[27–29] These findings demonstrate the presence of a variety of surface functional groups on GO, such as aromatic C–C stretching, quinine, phenolic, carboxylic, ethers and hydroxyl groups. These surface functional groups are essential to the surface chemistry of graphene oxide (GO), particularly when it comes to pollutant adsorption.

As shown in Fig. 1c, the XRD pattern identifies the phase formed in the obtained GO. The predominant wide diffraction observed at around 24° confirms the reflection in the (002) plane of aromatic layers. Furthermore, two peaks were observed at around 2θ equal to 43.3° and 44.6° corresponding to the (100) and (101) planes, respectively, indicating poly-crystalline characteristics of graphitic carbon.[30]

However, the Raman spectrum (Fig. 1d) shows the two distinctive peaks of graphitic carbon materials, G-band located at 1598 cm^{-1} which is attributed to the sp^2 hybridised carbon system and the D-band located at 1339 cm^{-1} is attributed to defects in the graphene layer.[25,26,29,31] Furthermore, the intensity ratio of the D and G bands (I_D/I_G), which quantify the relative levels of the disorder is 1.08, which confirmed that the obtained GO nanosheets have some sp^3 amorphous graphitic structure, which was confirmed from XPS analysis and TEM imaging (Fig. 1e), which shows GO as irregular transparent sheets above one another with some amorphous agglomeration as dark areas.

Fig. 1f displays the surface area of GO and the N_2 sorption isotherms for GO showed characteristic IUPAC-type III nature, exhibiting a narrow hysteresis loop and the amount of the N_2

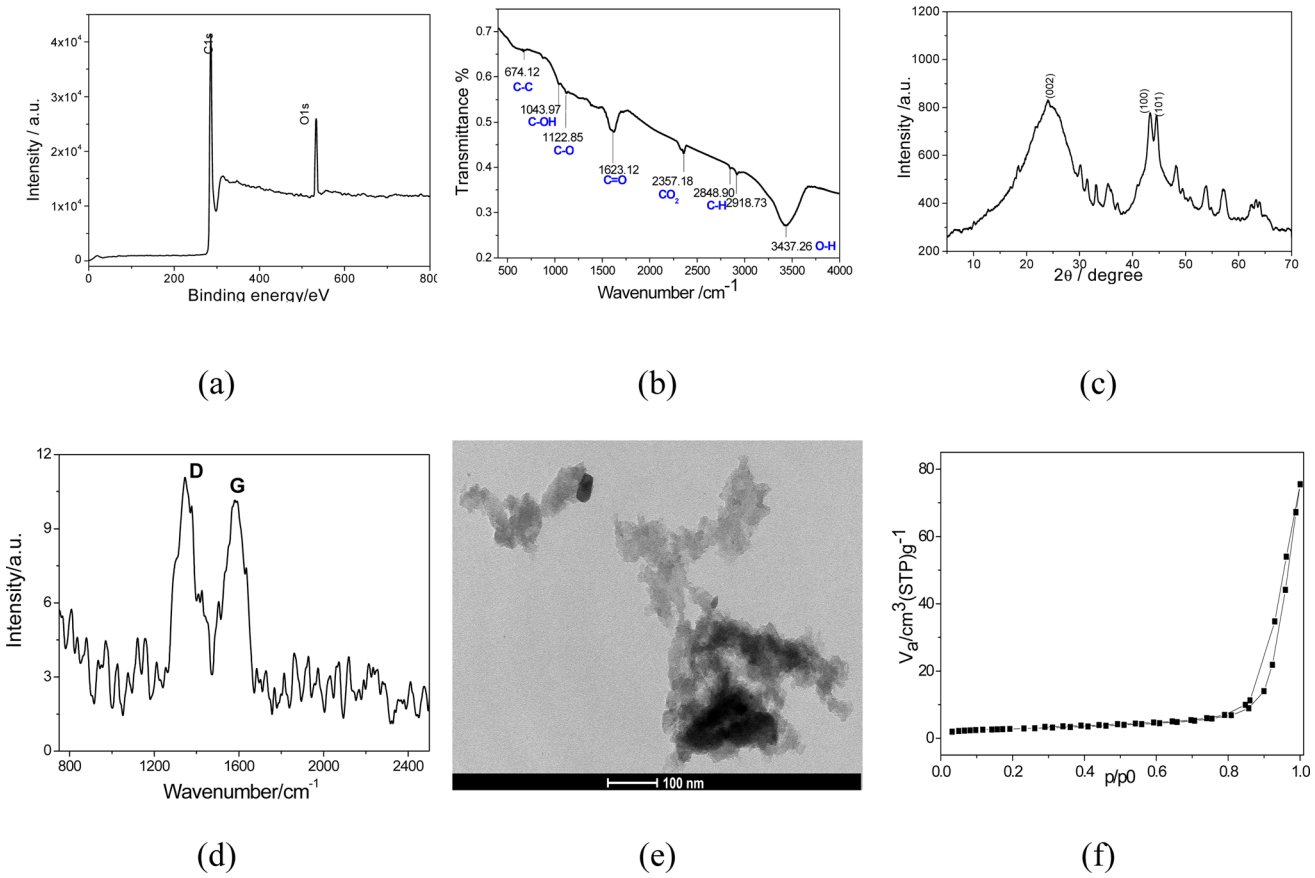

Fig. 1 (a) XPS survey spectrum, (b) FTIR spectrum, (c) XRD pattern (d) Raman spectrum, (e) TEM image and (f) N_2 adsorption–desorption isotherms for the prepared GO nanoparticles.

Table 2 Binding energy and assignment groups from C 1s and O 1s XPS spectra for GO

	Assignment groups	Binding energy
C 1s	C=C	283.9
	C–C	284.5
	C–OH	285.3
	C=O	287.1
	O–C=O	290.2
O 1s	C=O	530.5
	O–H, C–O–C	532.4
	C–O	533.5

adsorbed remains finite at the saturation pressure $p/p_0 = 1$, indicating the presence of meso- and macropores,[32] which has a positive effect on the adsorption process, in addition, the obtained GO has surface area of 20 m^2 g^{-1} which can provide numerous active sites for the adsorption process.

The characteristic properties of the GO@PVA coated films coated with different weight ratios of GO were investigated using different characteristic tools such as FTIR as shown in Fig. 2a. The stretching –OH groups of PVA, which constitute the primary constituent of the coated film, are characterised by board bands between 3078 and 3470 cm^{-1} in the FTIR spectra of GO@PVA coated films and crosslinked PVA films,[22] however the broad band around 2300 cm^{-1} is attributed to the C–H bonds in the PVA chain.[33] Every significant signal associated with the hydroxyl and acetate groups was detected as illustrated in the previous literature.[34] The effect of GO coating on the PVA spectra was noticed as a decrease in the peak intensity due to the hindring effect of GO coating and that confirmed the GO top layers on the PVA film.[35]

As shown in Fig. 2b, zeta potential values of GO, uncoated and coated films were found to decrease as pH increased from 3 to 12 because of their highly oxidised surfaces, which have many oxygen functionalities such as carboxylic and hydroxyl groups. These surfaces also make them more suitable for the adsorption process of cations in all environmental pH conditions.[36] The zeta potential of the GO_3@PVA coated film over the whole tested pH range (2–12) is lower than that for the other low GO concentration coated films and blank crosslinked PVA film, and that may be return to the GO_3@PVA coated film has the larger content of oxygenated groups.

Table S1 in the ESI† presents the findings of the investigation into the measurement of the contact angle. It was observed that all of the prepared films have contact angles less than 90° which means they have hydrophilic properties because GO has a large number of oxygenated functional groups. Additionally, it was observed that as GO content increased the coated films'

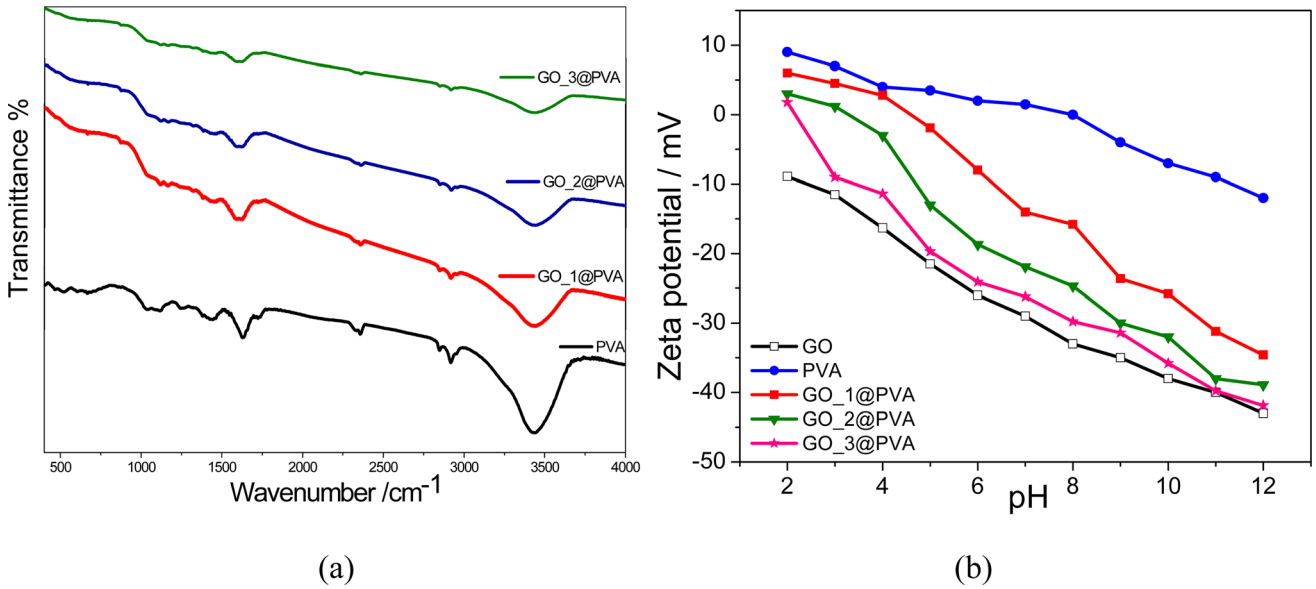

Fig. 2 (a) FTIR spectra, (b) zeta potentials based on different pH values.

contact angles decreased, and sequently, GO@PVA coated films' hydrophilicity increased. In the meantime, it is anticipated that GO_3@PVA coated films will display the lowest contact angle (Fig. 3a) and the highest activity during the adsorption process.

The SEM image for high GO concentration (3% wt) coated film shown in Fig. 3b demonstrates that the surface of the coated film shows nanoscale particles with low concentrations of aggregation.

3.2. Adsorption process evaluation

A batch adsorption process at solution pH of 7 and operating time of 180 min was conducted to examine the impact of varying the concentration of GO added to the PVA film on the MB and Pb^{2+} adsorption process. As shown in Fig. 4a the removal % of MB and Pb^{2+} by the prepared films increased as the GO content increased. This phenomenon can be explained by the formation of hydrogen bonds and a force of electrostatic attraction between the groups with positive charges in MB and Pb^{2+} ions and the oxygenated groups in the composite film. Furthermore, the adsorption capacity increased dramatically over time at first as shown in Fig. 4b, then steadily increased, after that period the adsorption process achieved equilibrium after about 150 minutes. This might be attributed to the equilibrium between the adsorption and desorption of MB cations and Pb^{2+} ions that occurs after this period, leading to the establishment of a steady-state condition.

This leads to 91.5 removal % and complete removal for MB and Pb, which is significantly higher compared to that by other PVA-based adsorbents reported in the literature (Table 3).

3.3. The impact of solution pH and adsorbent surface chemistry on the adsorption process

The GO_3@PVA coated film showed the highest hydrophilicity characterization and lowest zeta potential therefore it was used to investigate the effect of the solution pH on the adsorbent surface chemistry and the adsorption process. As mentioned above, the GO_3@PVA coated film contains many negatively charged groups, which makes them suitable for the adsorption

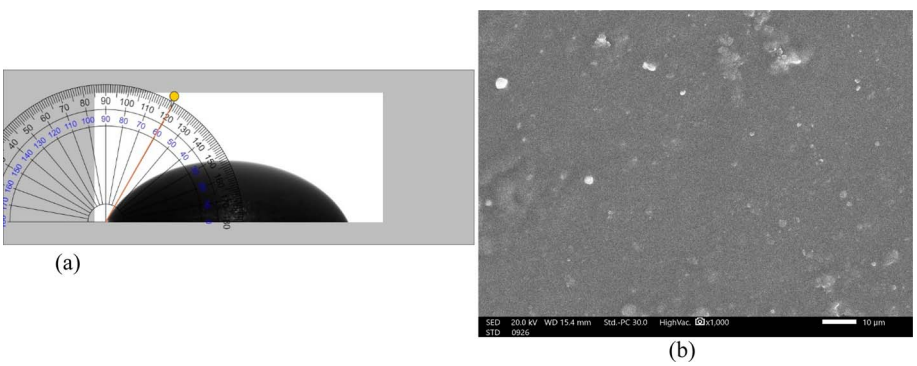

Fig. 3 (a) Contact angle measurement (b) SEM image of the top surfaces of GO_3@PVA coated films.

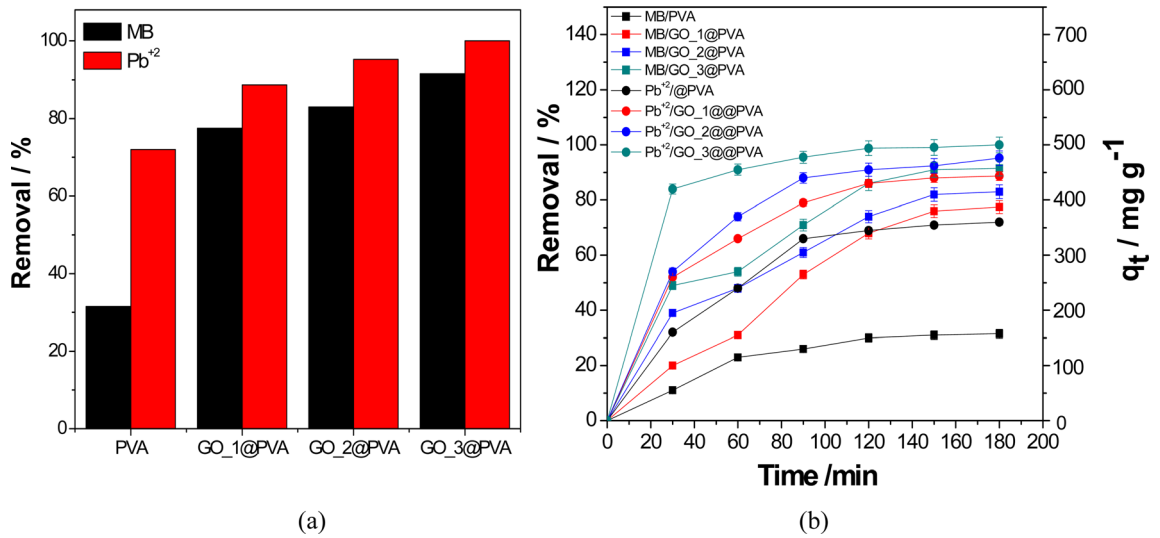

Fig. 4 (a) Effect of GO concentration and (b) effect of duration time on MB and Pb^{2+} adsorption process onto the GO_3@PVA coated film (at C_0 100 mg L^{-1}, film surface area 25 cm^2, temperature 25 °C, time (0–180) min, and volume 50 mL).

Table 3 A comparison between the performances of the proposed adsorbent with other commonly used adsorbents reported in the literature

Adsorbent	Adsorbate	Adsorbate initial concentration (mg L^{-1})	Adsorption time (min)	Efficiency (%)	Reference
PVA	MB	10	10	61.23	37
PVA/C_{dot}	MB	30	40	97	38
PVA/IC/PVP-3% SGO	MB	100	160	90.8	39
	GMS	100		94.7	
ZnO-PVA-coated membrane acidic environment (pH = 4)	Pb^{2+}	200	180	95	40
PVA/NH_2@TAtZnO composites	Pb^{2+}		400	92.8	41
GO_3@PVA	MB	100	180	91.5	This work
	Pb^{2+}	100	150	100	This work

of cations. Consequently, the impact of the solution pH on the adsorption of MB and Pb^{2+} onto the developed GO_3@PVA coated film was assessed within the range of 3 to 12. The elimination efficiency increased when the pH increased from 3 to 7, as shown in Fig. 5a. This phenomenon might be explained by the fact that several hydronium ions surround the GO_3@PVA film surface at low pH levels, competing with the cations of MB and Pb^{2+}. The hydroxyl and carboxylic groups in the coated film are fully ionised as a result of increase in the pH, and this also increases the electrostatic attraction between the film surface and the Pb^{2+} and MB cations, which gradually increases the effectiveness of the removal process. However, for Pb^{2+}, the adsorption process almost plateaus once pH increased to above 8 as at pH greater than 7, electrostatic repulsion makes it harder for lead hydroxides such as $Pb(OH)_2$ and $Pb(OH)_3^-$ to be adsorbed onto the negatively charged film surface, where it may readily form and precipitate.[6] Conversely, for MB cations, as the pH of the solution increases, the adsorption process increases because of the increase in the electrostatic attraction between the MB cations and the negatively charged GO_3@PVA film surface as shown in Fig. 5b. Therefore, a solution pH of 7 was selected as the optimum pH for removing Pb^{2+} in the other experiments while for MB the selected solution pH was 12. However, the adsorption mechanism of MB may be controlled by the adsorption sites and interactions such as hydrogen bonding of hydrophilic functional groups on the surface of the coated film, van der Waals forces, π–π conjugate and pore filling by filling the mesopores of the GO layer on the PVA film. While electrostatic interaction is the most probable mechanism affecting the adsorption of Pb^{2+}.[42]

3.4. Adsorption process optimization using the Box–Behnken design analysis

The process of adsorption was optimized through the application of a Box–Behnken design analysis. The temperature was kept at 25 °C. Quadratic dependency was assumed in order to represent the statistical link between variables and responses, namely the elimination % (Y), using the following equations:

$$Y_{MB} = 68.7 + 12.67A - 0.5625B + 33.71C - 5.7AB - + 6.15AC3 + 0.125BC - 2.69A^2 + 4.64B^2 - 15.01C^2 \quad (4)$$

$$Y_{Pb^{2+}} = 95.3 + 4.61A + 1.04B - 19.05C - 1.2AB - 2.47AC - 1.57BC + 3.7A^2 - 4.55B^2 - 66.78C^2 \quad (5)$$

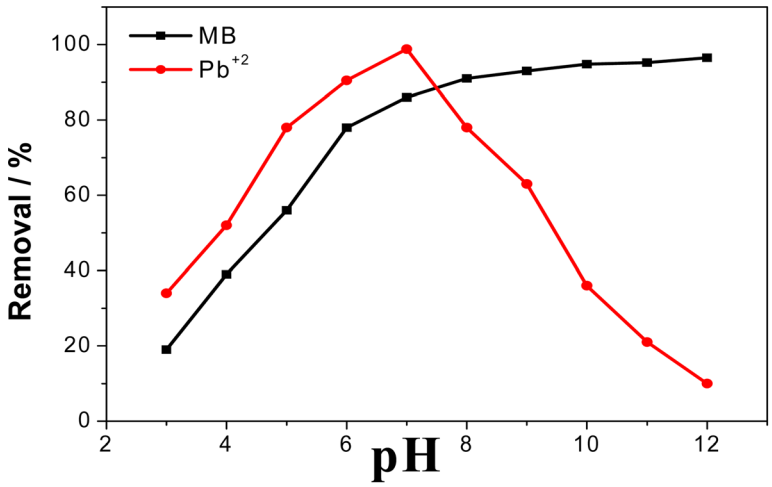

(a)

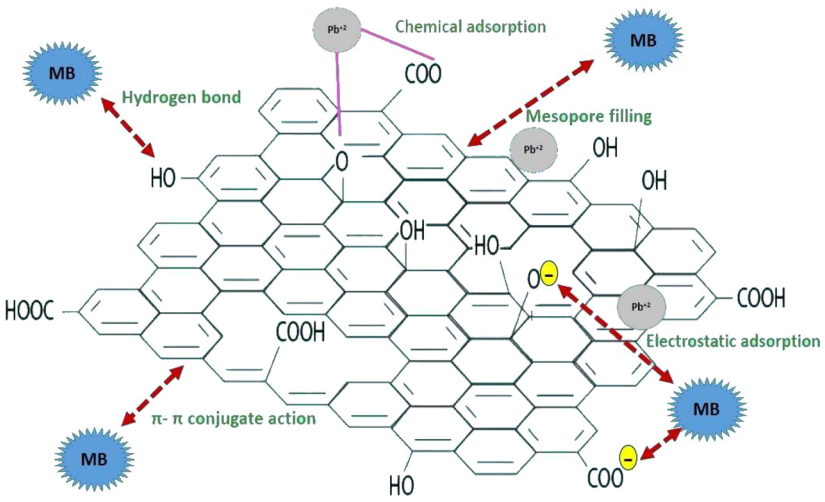

(b)

Fig. 5 (a) Solution pH effect on MB and Pb^{2+} adsorption onto the GO_3@PVA coated film, (b) different types of interactions involved in the adsorption of MB and Pb^{2+} onto the GO_3@PVA coated film.

where *A*, *B*, and *C* are the duration time, initial concentration of MB or Pb^{2+}, and the solution pH respectively (Table S2†).

For assessing the statistical significance of the quadratic response surface model, ANOVA analysis of variance is widely used. The quadratic model is a good fit for the high coefficient of determination R^2 (0.9807) for MB and (0.9911) for Pb^{2+}, as demonstrated in Tables S3 and S5.† It was determined that the quadratic model was significant because the *p*-value for MB and Pb^{2+} was less than 0.0001. It appeared that the following conditions would yield the best results: 180 min. of contact time, 113 mg L^{-1} of initial concentration, and a solution pH of 9 for MB to achieve 98% removal, and 150 min. of contact time, 155 mg L^{-1} of the initial concentration, and a solution pH of 6.5 for Pb^{2+}, in which case, complete removal was accomplished. The outcomes of the Box–Behnken design study are presented in the 3D surface plots shown in Fig. 6, which also illustrate the nature of the interactions between the variables that were investigated. The removal efficiency of MB seems to have decreased as initial concentrations increased from 100 to 150 mg L^{-1}, then increased again when MB concentration increased. This observation indicated that MB cations were initially adsorbed externally and that the adsorption rate increased again when MB cations competed to fill all active sides into GO_3@PVA. However, by increasing the contact time and solution pH the MB removal efficiency increased. In contrast, the removal efficiency of Pb^{2+} increases upon

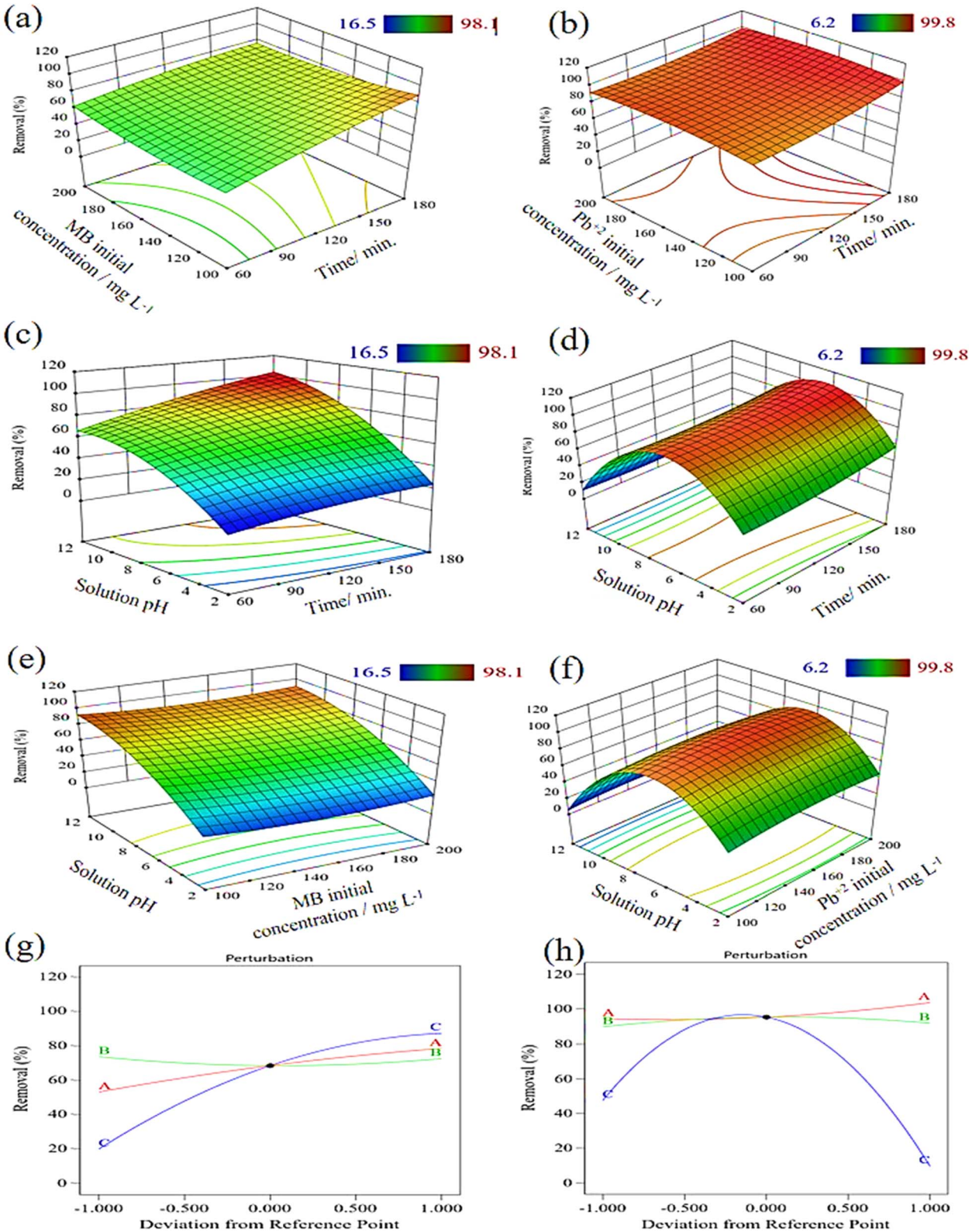

Fig. 6 3D surface (a)–(f) and perturbation plots (g and h) of MB and Pb^{2+} removal (%) on the prepared GO_3@PVA coated film.

increasing the contact time and decreases with an increase in the initial concentration. Meanwhile, as Fig. 6h demonstrates, the Pb^{2+} removal effectiveness is susceptible to variations in the solution pH whereas, the change in pH factor deviates more from the reference point than the other two components. Moreover, it was observed that the solution pH factor is the

most important factor that has a significant effect on the removal efficiency of MB dye and Pb^{2+} cations followed by the effect of time and the initial pollutant concentration.

3.5. Adsorption static kinetics

The kinetics investigation was significant since it clarified the adsorbate's uptake rate. Kinetic studies could provide light on the rate and mechanism of the MB and Pb^{2+} adsorption process onto the GO_3@PVA coated film. The pseudo-first-order and pseudo-second-order models were used to clarify the adsorption mechanism for different initial concentrations of 50, 100, and 150 mg L^{-1} for MB and Pb^{2+} at the solution pH of 9 for MB and solution pH of 6.5 for Pb^{2+} at 0.01 g weight of film and temperature of 25 °C, and solution volume of 50 mL. After 180 min and 150 min, the adsorption of MB and Pb^{2+}, respectively, on the prepared GO_3@PVA coated film reached equilibrium. Table 4 and Fig. S3† exhibit the relevant parameters and respective plots of the pseudo-first-order and pseudo-second-order models, respectively. When the adsorption capacities calculated using various models were compared to the experimental values, it was found that the pseudo-first-order model produced values that differed significantly from the experimental values, while the pseudo-second-order model produced values that agreed well with the experimental values, with a consistent higher correlation coefficient (R^2) than that for the pseudo-first-order model. The rate of adsorption for both MB and Pb^{2+} was dictated by the accessibility of the adsorption sites on the adsorbent surface, and chemisorption was the rate-limiting phase since the adsorption closely matched the pseudo-second-order model.

3.6. Adsorption–desorption tests

The structural stability and reusability of the GO_3@PVA coated film were evaluated during five adsorption–desorption cycles. It turned out that even with this continued use, the removal efficacy remained strong, as shown in Fig. 7, with each desorption stage, the removal efficiency was slightly reduced. This bodes well for the possible implementation of the coated film's large-scale industrial manufacturing in real water filtration systems.

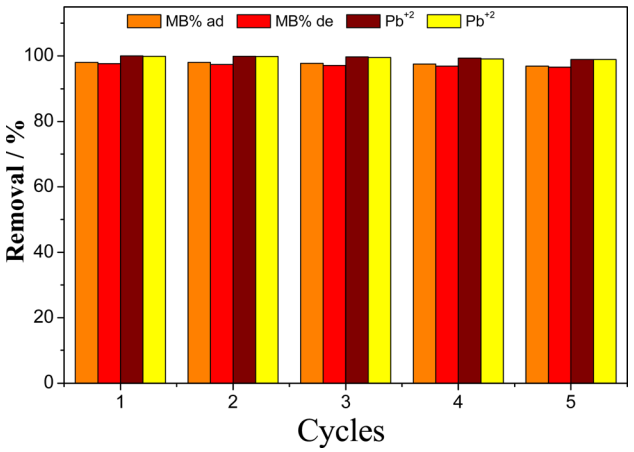

Fig. 7 Reusability cycles of MB and Pb^{2+} into the GO_3@PVA coated film with a film area of 25 cm^2, an initial concentration of 20 mg L^{-1} at pH 9 for MB and pH 6.5 for Pb^{2+}, and a temperature of 25 °C.

Table 4 Kinetic models' parameters and determination coefficients for MB and Pb^{2+} adsorption onto the GO_3@PVA film at a solution pH of 9 for MB and solution pH of 6.5 for Pb^{2+} removal

Initial concentrations (mg L^{-1}) adsorbed onto the GO_3@PVA nanocomposite film						
	50		100		150	
	MB	Pb^{2+}	MB	Pb^{2+}	MB	Pb^{2+}
$q_{e,exp}$ (mg g^{-1})	178	368	386	447	456	508
Pseudo-1st-order						
$q_{e,cal}$ (mg g^{-1})	12.1	10.38	16.43	16.5	21.18	21.2
k_1 (min^{-1})	0.03	0.08	0.007	0.11	0.11	0.11
R^2	0.79	0.67	0.62	0.91	0.75	0.77
Pseudo-2nd-order						
$q_{e,cal}$ (mg g^{-1})	247	258	536	489	448	646
k_2 (min^{-1})	0.004	0.004	0.002	0.002	0.002	0.001
R^2	0.995	0.97	0.993	0.998	0.951	0.998

4. Conclusions

Novel coated films for wastewater treatment were fabricated using crosslinked PVA films coated with different ratios of GO which were obtained through the catalytic pyrolysis of flexographic printing plates wastes. The coated films were examined for the removal of MB and Pb^{2+} cations after being characterised in terms of their morphology and content. It was determined that the interactions between the different functional groups of PVA and GO inside the composite film and the functional groups of MB and Pb^{2+} ions controlled the chemistry of the adsorption process. The RSM design was used to optimize the MB and Pb^{2+} removal efficiency using the GO_3@PVA film, which exhibits the highest hydrophilicity property and lowest zeta potential values. The GO_3@PVA coated film absorbance was analyzed using various kinetic models to shed light on the removal mechanism. It was discovered that the functional groups in the film and the pollutants' molecules combined to chemisorb and adsorb electrostatically. Five consecutive cycles of excellent coated film absorption and desorption were observed as an additional means of demonstrating strong reusability.

Data availability

The data supporting this article have been included as part of the ESI.†

Author contributions

Noha A. Elessawy: conceptualization, formal analysis, investigation, visualization, writing – original draft. Abdulrahman G. Alhamzani: investigation, visualization, writing – original draft.

Mortaga M. Abou-Krisha: investigation, writing – original draft. Saad Aljlil: validation, writing – review and editing.

Conflicts of interest

The authors declare no competing interests.

Acknowledgements

The authors acknowledge Inciflex Egypt for Industry and Trade Co. for providing this research with flexographic printing waste plates.

References

1 N. A. El Essawy, A. H. Konsowa, M. Elnouby and H. A. Farag, A novel one-step synthesis for carbon-based nanomaterials from polyethylene terephthalate (PET) bottles waste, *J. Air Waste Manage. Assoc.*, 2017, **67**, 358–370.

2 N. A. Elessawy, M. H. Gouda, S. M. Ali, M. Salerno and M. S. M. Eldin, Effective elimination of contaminant antibiotics using high-surface-area magnetic-functionalized graphene nano-composites developed from plastic waste, *Materials*, 2020, **13**, 1517.

3 N. A. Elessawy, M. H. Gouda, M. F. Elkady, S. M. Ali, M. Gouda and M. S. M. Eldin, Ultra-fast removal of cadmium and lead from wastewater using high-efficient adsorbent derived from plastic waste: statistical modeling, kinetic and isotherm studies, *Desalin. Water Treat.*, 2020, **173**, 394–408.

4 E. M. Elsayed, M. Elnouby, M. H. Gouda, N. A. Elessawy and D. M. F. Santos, Effect of the morphology of tungsten oxide embedded in sodium alginate/polyvinylpyrrolidone composite beads on the photocatalytic degradation of methylene blue dye solution, *Materials*, 2020, **17**, 1905.

5 S. Ata, A. Tabassum, I. Bibi, F. Majid, M. Sultan, S. Ghafoor, M. A. Bhatti, N. Qureshi and M. Iqbal, Lead Remediation Using Smart Materials. A Review, *Z. Phys. Chem.*, 2019, **233**, 1377–1409.

6 K. Chen, J. He, Y. Li, X. Cai, K. Zhang, T. Liu, Y. Hu, D. Lin, L. Kong and J. Liu, Removal of cadmium and lead ions from water by sulfonated magnetic nanoparticle adsorbents, *J. Colloid Interface Sci.*, 2017, **494**, 307–316.

7 M. Abujazar, S. Karaăgaç, S. Abu Amr, M. Alazaiza and M. Bashir, Recent advancement in the application of hybrid coagulants in coagulation-flocculation of wastewater: areview, *J. Cleaner Prod.*, 2022, **345**, 131133.

8 S. Ihaddaden, D. Aberkane, A. Boukerroui and D. Robert, Removal of methylene blue (basic dye) by coagulation-flocculation with biomaterials (bentonite and Opuntia ficus indica), *J. Water Process Eng.*, 2022, **49**, 102952.

9 M. Z. Alam, M. J. H. Khan, N. A. Kabbashi and S. M. A. Sayem, Development of an effective biosorbent by fungal immobilization technique for removal of dyes, *Waste Biomass Valorization*, 2018, **9**, 681–690.

10 M. Sagaseta de Ilurdoz, J. J. Sadhwani and J. V. Reboso, Antibiotic removal processes from water & wastewater for the protection of the aquatic environment – a review, *J. Water Process Eng.*, 2022, **45**, 102474.

11 A. Mirzaei, F. Haghighat, Z. Chen and L. Yerushalmi, Sonocatalytic removal of ampicillin by Zn(OH)F: effect of operating parameters, toxicological evaluation and by-products identification, *J. Hazard. Mater.*, 2019, **375**, 86–95.

12 S. Mazhar, U. Y. Qazi, N. Nadeem, M. Zahid, A. Jalil, F. Khan, I. Ul-Hasan and I. Shahid, Photocatalytic degradation of methylene blue using polyaniline-based silver-doped zinc sulfide (PANI-Ag/ZnS) composites, *Environ. Sci. Pollut. Res.*, 2022, **29**, 9203–9217.

13 G. Yang, D. Bao, D. Zhang, C. Wang, L. Qu and H. Li, Removal of antibiotics from water with an all-carbon 3D nanofiltration membrane, *Nanoscale Res. Lett.*, 2018, **13**, 146.

14 D. Mangla, Annu, A. Sharma and S. Ikram, Critical review on adsorptive removal of antibiotics: present situation, challenges and future perspective, *J. Hazard. Mater.*, 2022, **425**, 127946.

15 Q. Cheng, Q. Huang, S. Khana, Y. Liua, Z. Liao, G. Li and Y. OK, Adsorption of Cd by peanut husks and peanut husk biochar from aqueous solutions, *Ecol. Eng.*, 2016, **87**, 240–245.

16 L. Leng, X. Yuan, G. Zeng, J. Shao, X. Chen, Z. Wua, H. Wanga and X. Peng, Surface characterization of rice husk bio-char produced by liquefaction and application for cationic dye (Malachite green) adsorption, *Fuel*, 2015, **155**, 77–85.

17 B. Li, L. Yang, C. Wang, Q. Zhang, Q. Liu, Y. Li and R. Xiao, Adsorption of Cd(II) from aqueous solutions by rape straw biochar derived from different modification processes, *Chemosphere*, 2017, **175**, 332–340.

18 M. Samy, M. Elkady, A. Kamal, N. Elessawy, S. Zaki and M. Eltarahony, Novel Biosynthesis of Graphene-Supported Zero-Valent Iron Nanohybrid for Efficient Decolorization of Acid and Basic Dyes, *Sustainability*, 2022, **14**, 14188.

19 A. Toghan, M. H. Gouda, H. F. Zahran, A. I. Alakhras, M. Sanad and N. A. Elessawy, Development of a new promising nanocomposite photocatalyst of polyaniline/carboxylated graphene oxide supported on PVA film to remove different ecological pollutants, *Diamond Relat. Mater.*, 2023, **139**, 110400.

20 W. Shi, X. Zeng, H. Li, R. Li, H. Zhang and X. Qin, Preparation of carboxylated gra-phene oxide nanosheets/polysulphone hollow fibre separation membranes with improved separation and dye adsorption properties, *Color. Technol.*, 2019, **135**, 370–382.

21 M. Gouda, A. H. Konsowa, H. Farag, N. A. Elessawy, T. M. Tamer and M. S. Mohy Eldin, Novel nanocomposite membranes based on cross-linked eco-friendly polymers doped with sulfated titania nanotubes for direct methanol fuel cell application, *Nanomater. Nanotechnol.*, 2020, **10**, 1–9.

22 M. H. Gouda, N. A. Elessawy and D. M. F. Santos, Synthesis and Characterization of Novel Green Hybrid Nanocomposites for Application as Proton Exchange Membranes in Direct Borohydride Fuel Cells, *Energies*, 2020, **13**, 1180.

23 G. Box and D. Behnken, Some new three level designs for the study of quantitative varia-bles, *Technometrics*, 1960, **2**, 455–475.

24 N. A. Elessawy, A. Toghan, M. S. Elnouby, A. Alakhras, H. A. Hamad and M. E. Youssef, Development and activity enhancement of zirconium/vanadium oxides as micro-heterogeneous ceramic electrocatalyst for ORR in low temperature fuel cell, *Ceram. Int.*, 2023, **49**, 4313–4321.

25 M. M. Viana, M. C. F. S. Lima, J. C. Forsythe, V. S. Gangoli, M. Cho, Y. Cheng, G. G. Silva, M. S. Wong and V. Caliman, Facile graphene oxide preparation by microwave-assisted acid method, *J. Braz. Chem. Soc.*, 2015, **26**, 978–984.

26 V. R. Moreira, Y. A. R. Lebron, M. M. da Silva, L. V. Santos, R. S. Jacob, C. K. de Vasconcelos and M. M. Viana, Graphene oxide in the remediation of norfloxacin from aqueous matrix: simultaneous adsorption and degradation process, *Environ. Sci. Pollut. Res.*, 2020, **27**, 34513–34528.

27 Y. Gong, D. Li, Q. Fu and C. Pan, Influence of graphene microstructures on electrochemical performance for supercapacitors, *Prog. Nat. Sci.: Mater. Int.*, 2015, **25**, 379–385.

28 K. Tian, Z. Su, H. Wang, X. Tian, W. Huang and C. Xiao, N-doped reduced graphene oxide/waterborne polyurethane composites prepared by in situ chemical reduction of graphene oxide, *Composites, Part A*, 2017, **94**, 41–49.

29 Sudesh, N. Kumar, S. Das, C. Bernhard and G. D. Varma, Effect of graphene oxide doping on superconducting properties of bulk MgB2, Supercond, *Sci. Technol.*, 2013, **26**, 095008.

30 T. Qiu, J. Yang, X. Bai and Y. Wang, The preparation of synthetic graphite materials with hierarchical pores from lignite by one-step impregnation and their characterization as dye absorbents, *RSC Adv.*, 2019, **9**, 12737–12746.

31 N. Elessawy, M. Abdel Rafea, N. Roushdy, M. Youssef and M. H. Gouda, Development and evaluation of cost-effective and green Bi-functional nickel oxide decorated graphene electrocatalysts for alkaline fuel cells, *Results Eng.*, 2023, **17**, 100871.

32 M. Thommes, K. Kaneko, A. V. Neimark, J. P. Olivier, F. R. Reinoso, J. Rouquerol and K. S. W. Sing, Physisorption of gases, with special reference to the evaluation of surface area and pore size distribution (IUPAC Technical Report), *Pure Appl. Chem.*, 2015, **87**, 1051–1069.

33 K. Deshmukh, M. B. Ahamed, K. K. Sadasivuni, D. Ponnamma, R. R. Deshmukh, S. K. K. Pasha, M. A. AlMaadeed and K. Chidambaram, Graphene oxide reinforced polyvinyl alcohol/polyethylene glycol blend composites as high-performance dielectric material, *J. Polym. Res.*, 2016, **23**, 1–13.

34 H. S. Mansur, C. M. Sadahira, A. N. Souza and A. A. P. Mansur, FTIR spectroscopy characterization of poly(vinyl alcohol) hydrogel with different hydrolysis degree and chemically crosslinked with glutaraldehyde, *Mater. Sci. Eng. C*, 2008, **28**, 539–548.

35 F. Baskoro, C. Wong, S. R. Kumar, C. Chang, C. Chen, D. W. Chen and S. Lue, Graphene oxide-cation interaction: inter-layer spacing and zeta potential changes in response to various salt solutions, *J. Membr. Sci.*, 2018, **554**, 253–263.

36 B. Jun, J. Heo, N. Taheri-Qazvini, C. M. Park and Y. Yoon, Adsorption of selected dyes on Ti3C2Tx MXene and Al-based metal-organic framework, *Ceram. Int.*, 2020, **46**, 2960–2968.

37 S. Agarwal, H. Sadegh, M. Monajjemi, A. S. Hamdy, G. A. M. Ali, A. O. H. Memar, R. Shahryari-ghoshekandi, I. Tyagi and V. K. Gupta, Efcient removal of toxic bromothymol blue and methylene blue from wastewater by polyvinyl alcohol, *J. Mol. Liq.*, 2016, **218**, 191–197, DOI: **10.1016/j.molliq.2016.02.060**.

38 A. G. El-Shamy and H. S. S. Zayied, New polyvinyl alcohol/carbon quantum dots (PVA/CQDs) nanocomposite films: structural, optical and catalysis properties, *Synth. Met.*, 2020, **259**, 116218, DOI: **10.1016/j.synthmet.2019.116218**.

39 M. H. Gouda, M. M. Khowdiary, H. Alsnani, N. Roushdy, M. E. Youssef, M. Elnouby and N. A. Elessawy, Adsorption and antibacterial studies of a novel hydrogel adsorbent based on ternary eco-polymers doped with sulfonated graphene oxide developed from upcycled plastic waste, *J. Contam. Hydrol.*, 2024, **264**, 104362.

40 H. M. Rasheed, A. Rauf, M. Arif, A. Mohyuddin, M. Javid, S. Nadeem, A. Yousuf, M. Irfan, S. M. Haroon, H. Raza, S. M. Ibrahim and S. Ul Mahmood, Selective Removal of Lead (II) Ions from Wastewater with Fabricated ZnO-PVA Membrane, *JOM*, 2023, **75**, 5310–5320, DOI: **10.1007/s11837-023-05957-6**.

41 L. Liu, S. Xu, Z. Wang, X. Chen, M. Cao, S. Zhang, Y. Liu and J. Cui, Building of soft-hard compound brush in porous PVA/NH2@TAtZnO plural gel and the high-efficiency anti-interference removal on Pb(II), *Chemosphere*, 2023, **319**, 137990, DOI: **10.1016/j.chemosphere.2023.137990**.

42 A. Chakraborty, S. Bhattacharyya, A. Hazra, A. C. Ghosh and K. Maji, Post-synthetic metalation in an anionic MOF for efficient catalytic activity and removal of heavy metal ions from aqueous solution, *Chem. Commun.*, 2016, **52**, 2831–2834, DOI: **10.1039/C5CC09814A**.